



Platinum nanoparticles supported on nitrogen-doped carbons as electrocatalysts for oxygen reduction reaction

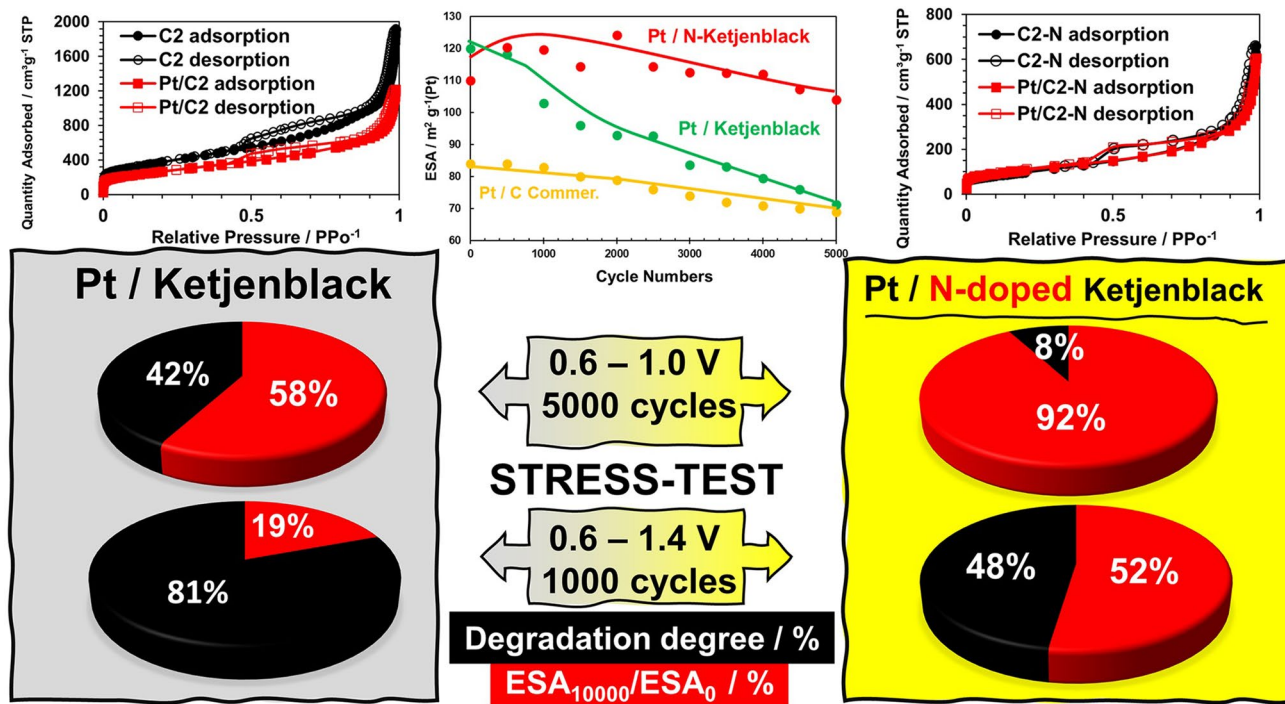
E. A. Moguchikh¹ · K. O. Paperzh¹ · A. A. Alekseenko¹ · E. N. Gribov^{2,3} · N. Yu. Tabachkova⁴ · N. V. Maltseva^{2,3} · A. G. Tkachev⁵ · E. A. Neskromnaya⁵ · A. V. Melezhik⁵ · V. V. Butova⁶ · O. I. Safronko¹ · V. E. Guterman¹

Received: 19 March 2021 / Accepted: 25 September 2021
© The Author(s), under exclusive licence to Springer Nature B.V. 2021

Abstract

Behavior of Pt/C catalysts obtained by the platinum deposition on standard and nitrogen-doped carbon supports with different microstructure has been studied in the oxygen electroreduction reaction in an acidic electrolyte. The catalysts based on the modified supports are characterized by a uniform spatial distribution of small-sized (1.5–2 nm) Pt nanoparticles over the surface of the supports, which results in high values of the electrochemically active surface area (110–130 m² g⁻¹ (Pt)). The use of various stress testing protocols has shown that the Pt/C material based on the N-doped KetjenBlack EC DJ-600 possesses the highest mass activity and durability, which noticeably exceed the corresponding characteristics of the commercial HiSPEC3000 catalyst.

Graphic abstract



Keywords Nitrogen-doped carbon · Pt catalysts · Oxygen reduction reaction · Durability · Catalyst activity · Catalyst stability · Catalyst preparation · Catalyst performance · Catalyst lifetime

Extended author information available on the last page of the article

1 Introduction

Porous carbon materials are most often used as supports for platinum-containing electrocatalysts used in PEM FC [1–3]. The main requirements for the electrocatalysts support are high surface area, optimal porosity, which allows reagents to supply and remove the products of current-forming reactions to/from the platinum nanoparticles or its alloys, high electronic conductivity, and sufficient corrosion resistance under PEM FC operating conditions [3–5]. One of the most widely used supports is Vulcan XC-72 carbon black [6, 7]. This is due to its high availability, low cost, optimal combination of size, shape, surface area, and porosity of the carbon particles. Nevertheless, the search for supports that would make it possible to obtain Pt/C catalysts more resistant to degradation as compared to Pt/Vulcan XC-72 is very urgent nowadays [8]. Moreover, it is assumed that the development of new carbon materials with special physicochemical properties can lead to an increase not only in the stability, but also in the activity of Pt/C catalysts [9–11]. The most serious problem is the degradation of Pt/C catalysts on the PEM FC oxygen electrode, where highly active oxygen-containing intermediates are formed in the process of multistage electroreduction of O₂ molecules [8].

The set of Pt/C degradation mechanisms can, with some approximation, be reduced to two groups of processes [12]. The first group includes phenomena associated with certain transformations of platinum nanoparticles: corrosive dissolution, Ostwald ripening, and/or aggregation of nanoparticles. The primary cause of the processes in the second group is the degradation of the carbon support itself, which occurs mainly at the carbon/Pt interface and is catalyzed by platinum itself [6, 8, 12, 13].

The search for more stable carbon supports, such as graphitized or modified carbon materials [14], carbon nanotubes [15], or various types of graphene [15, 16], takes an important place among various attempts to solve the problem of the Pt/C catalysts durability. The high surface area of graphene sheets (more than 2600 m² g⁻¹), structural perfection, and excellent electronic conductivity make it a very promising material for use as catalyst support [17]. The main problem is that graphene easily agglomerates due to interactions between its individual layers, especially in the manufacture of powder materials. As a result, there are problems of the uniform deposition of noble metal nanoparticles on graphene sheets [17, 18]. Platinum catalysts based on carbon nanotubes can demonstrate higher stability compared to the ones conventionally used on the carbon black supports [19]. The adhesion of platinum NPs to the nanotube surface can be improved by creating artificial defects or intercalation of heteroatoms into

the structure of graphene layers [19]. Similar approaches can be used for graphene. Nevertheless, the high cost of producing carbon nanotubes, as well as the problems of their aggregation during the formation of the porous Pt/C layers, do not allow considering this type of carriers as the promising materials for commercial use in the creation of electrocatalysts.

Recently, among the researchers, there has been a growing interest in increasing the stability of “ordinary” dispersed carbon materials due to the doping of their surface layers with N, B, P, and S heteroatoms [20–22]. To a large extent, these studies were initiated by the perspective of developing platinum-free electrocatalysts for the oxygen electroreduction (ORR) reaction in alkaline electrolytes. The active centers of catalysis in such materials can be groups containing heteroatoms, for example, nitrogen atoms linked to carbon by pyrrole and/or pyridine bonds [21, 23]. At the same time, in a number of publications, it has been reported that doping of carbon with heteroatoms can lead to an increase in the stability of supported platinum electrocatalysts ORR in acidic electrolytes [19–21]. Since heteroatoms in any case intercalate into the graphene layers of the support, it is convenient to study their influence namely on graphene, and then extrapolate the result to the particles of the carbon material, which are larger in size and more complex in organization. For example, it was found that doping of graphene with nitrogen leads to an increase in the binding energy of the precious metal nanoparticles with the substrate [24–26]. The atomic radius of N (70 pm) and carbon C (77 pm) are very close. This means that the N atom can replace the C atom, and it is relatively easy to penetrate into the structure of the graphene layer. Due to strong covalent N–C interactions, the structure of N-doped carbon is more stable [27]. Intercalation of nitrogen into carbon, as a rule, is carried out at high temperatures and can be accompanied by carbon graphitization [21]. Graphitization itself can also increase the stability of the support and support platinum catalysts [28, 29]. At the same time, the processes of the heteroatoms intercalation into the carbon structure, accompanied by an increase in the degree of graphitization, lead to a decrease in the support surface area; therefore, carbon materials with an initially high surface area are used for modification [30].

It should be noted that electrocatalysts based on N-doped carbon carriers make it possible to form a uniform catalytic layer during the assembly of membrane-electrode blocks (MEA) of fuel cells. Due to the Coulomb interaction of Nafion- and nitrogen-containing groups on the catalyst surface, the oxygen distribution and proton supply to platinum nanoparticles are improved [20]. Researchers emphasize such important characteristics of carbon carriers as the ratio of meso-, micro-, and macropores, and they point out the effect of N-doping on the change in the pore size [3]. It was established in [3] that a decrease in the fraction of

micropores in carbon support allows one to reduce the resistance associated with O₂ transport during operation of a fuel cell, while minimizing the volume of macropores contributes to a more uniform distribution of a thin ionomer film, thus ensuring a better proton transfer. The change in the ratio of pores of different sizes in carbon grades Vulcan XC-72 [21] and Ketjenblack [31] can be achieved precisely due to N-doping of the initial carbon carriers at high temperatures.

In this work, we have studied the activity in the oxygen electroreduction (ORR) reaction and the stability in acidic electrolytes of platinum-containing electrocatalysts based on new N-doped carriers: nitrogen-doped graphitized carbon KetjenBlack EC DJ-600 and N-doped graphene. Well-known commercial catalyst HiSPEC3000 (Johnson Matthey) and the Pt/C catalyst based on the undoped support KetjenBlack EC DJ-600, platinum being deposited on them in the same way as on two nitrogen-modified supports, were investigated as reference samples. The study was based on the hypothesis that modification of carbon carriers with nitrogen atoms will lead to the strengthening of the adhesion of platinum nanoparticles, which will positively affect the stability and, highly likely, the activity of the catalyst.

2 Experimental

2.1 Materials synthesis

2.1.1 Synthesis of modified carriers

Modification of the KetjenBlack EC DJ-600 support with nitrogen was carried out according to the procedure described in [30]. Acetonitrile was used as a nitrogen source. A sample of the support was loaded into a U-shaped quartz reactor. Argon saturated at room temperature with acetonitrile vapor was passed through a carbon-supported reactor at temperature 890 °C with a flow rate of 0.4 cm³ s⁻¹ for 4 h. The procedure was repeated several times to produce the modified support – C1N. It was shown before that nitrogen on the support surface is present mainly in the pyridinic and pyrrolic forms [30].

Reduced graphene oxide [know-how technology of the NanoTechCenter LLC (Tambov, Russia)] was used to obtain the C2N carbon support (graphene-like N-doped carbon support). It consisted of smooth graphene flakes (Fig. S1), mass composition: C = 80.9%, N = 13.1%, O = 6.0%. This material was carbonized in an argon atmosphere for 1 h at 800 °C, resulting in a carbon support, in the work referred to as C2N (graphene-like N-doped carbon support).

Note, information on the synthesis of similar materials is available in literature [32–34].

2.1.2 Synthesis of Pt/C catalysts

The preparation of Pt/C catalysts was carried out by chemical reduction of platinum from a solution of H₂PtCl₆·6H₂O (TU 2612-034-00205067-2003, mass fraction of Pt 37.6%, Aurat, Russia). The carrier were KetjenBlack EC DJ-600 (C1) carbon material and two nitrogen-doped carbon carriers—KetjenBlack EC DJ-600-N (C1N) and a graphene-like N-doped carbon carrier (C2N).

A 0.15 g weighed portion of carbon support was placed in 18 cm³ of ethylene glycol (premium grade, no less than 99.8%wt., Reakhor Lls., Russia). The suspension was stirred on a magnetic stirrer for 15 min, after that it was sonicated in a homogenizer for 1 min at an amplitude of 50% and a power of 750 W. Then, with constant stirring, a calculated amount of hydrochloric acid solution with a concentration of 17.9 mg (Pt) cm⁻³ was added, stirred for 5 min, and 0.5 M NaOH (n(OH)/n(Pt) = 12) was added. The mixture was transferred to a 100 ml round bottom flask. With constant stirring, 1 ml of formaldehyde (premium, 37.2%wt., GOST 1625-89, Russia) was added. Then, in an inert atmosphere, the temperature was increased to 80 °C and the reaction mixture was kept under constant stirring for 2 h. After spontaneous cooling of the suspension for 40 min, the product was filtered and washed repeatedly with portions of isopropyl alcohol and bidistilled water. The catalysts were kept for 1 h in an oven at 80 °C, then for 12 h in a desiccator over P₂O₅.

Taking into account the nature of the support, the obtained catalysts are marked below as E1, E1N, E2N. A commercial HiSPEC3000 platinum-carbon catalyst (Johnson Matthey, 20%wt. Pt), designated JM, was used as a reference one.

2.2 Materials characterizations

2.2.1 Methods for studying the composition and structure of materials

The ω(Pt), Pt-loading in the obtained materials, was determined by the mass of the residue (Pt) after their combustion (800 °C, 40 min). The measurement accuracy was ± 3% of the measured ω(Pt) value (Table 1). The calculated loading of platinum in catalysts is 23%wt.

X-ray diffraction patterns of carbon carriers and Pt/C materials were recorded in the 2-theta angle range of 15–55 degrees on an ARL X'TRA diffractometer (Thermo Scientific, Switzerland) using filtered CuKα radiation (λ = 0.154056 nm) at room temperature. The average crystallite size of Pt was calculated according to Scherer's equation, this procedure was described earlier in [35]. The measurement accuracy was ± 9% (Table 1).

The average size of platinum nanoparticles, the peculiarities of their size and spatial distributions were also studied

Table 1 Composition and structural characteristics of carbon supports and Pt/C electrocatalysts

Sample	Carbon support type	Support surface area, S(C), m ² g ⁻¹	Pt-loading, ω , %wt.	Average crystallite size of Pt, nm (XRD) ^a	Average size of Pt NPs, nm (TEM)
E1	Ketjenblack EC DJ-600	1352	20	Less than 1.0	1.5
E1N	Ketjenblack EC DJ-600-N	345	22	Less than 1.0	2.0
E2N	Graphene-like N-doped carbon support	270	23	1.3	1.8
JM	–	184 [42]	20	2.4	2.8

^aDetermination of the average crystallite size according to the Scherrer equation based on the analysis of X-ray diffraction patterns for some samples was difficult because of the Pt (111) peak broadening due to the small crystallite size

by TEM. TEM photographs were obtained using a JEM-2100 microscope (JEOL, Japan) at a voltage of 200 kV and a resolution of 0.2 nm. For measurements, a suspension of each sample in isopropanol was prepared in a special way and the investigation was carried out as described in more detail in [36]. The histograms of the size distribution of platinum nanoparticles in the catalysts were constructed based on determining the sizes of at least 400 particles randomly selected in the TEM images.

Nitrogen adsorption-desorption isotherms were measured at – 96 °C on Accelerated Surface Area and Porosimetry analyzer ASAP 2020 (micromeritics). The samples were evacuated at 90 °C to achieve pressure 100 μ mHg, then heated up to 150 °C with the rate of 0.5 ° min⁻¹ and activated at this temperature for 10 h under a dynamic vacuum before the measurement. The specific surface area values were calculated according to the BET model [37]. Pore volume was determined at a relative pressure of 0.97. Pore size distribution was estimated by original density functional theory (DFT) according to the model of carbon with slit pores.

All XPS spectra were obtained on the ESCALAB 250 X-ray photoelectron spectrometer using monochromatic X-ray radiation Al K α - line with an energy of 1486.6 eV. The minimum range of the resolved energy determined from the Ag 3d_{5/2,3/2} doublet, did not exceed 0.6 eV. The spectra were processed using the built-in Avantage™ software. As part of the spectra processing, the background was subtracted using the Smart form, the XPS lines were approximated by L/G Mix functions (30% Lorencian, 70% Gaussian). Samples in a powdery state were deposited on Carbon Tape, which was attached to a standard sample holder of the spectrometer.

2.2.2 Electrochemical methods

Catalytic ink was used to apply a thin layer of a catalyst to a glass graphite electrode. A detailed description of the preparation of the catalytic ink system is given in the Supplementary Information. Cyclic voltammograms (CV) were recorded on a VersaSTAT3 potentiostat in a three-electrode cell filled with a 0.1 M HClO₄ solution saturated with Ar at

the atmospheric pressure at 25 °C. Ag/AgCl/KCl saturated electrode was used as a reference electrode, Pt wire—as an auxiliary electrode. Before the electrode under study was immersed in an electrolyte solution, its surface was moistened with 0.1 M HClO₄. All potentials in this work are given relative to RHE.

Initially, electrochemical activation (standardization) of the electrode surface was carried out [35]. Then, 2 CVs were recorded in the same potential range at a sweep rate of 20 mV s⁻¹. The electrochemically active surface area of the catalysts (ESA) was estimated for the second cyclic voltammogram by the half-sum of the amounts of electricity consumed for electrochemical adsorption (Q_{ad}) and desorption (Q_d) of atomic hydrogen in the process of CV measurement.

Additionally, ESA was also determined from the electrochemical desorption of a CO monolayer, as described in [38]. A detailed calculation of the platinum ESA based on hydrogen adsorption/desorption and CO desorption is given in Supplementary Information. The ESA determination accuracy was \pm 10% (Table 2).

To determine the catalysts activity in the ORR, we measured a series of voltammograms with a linear potential sweep (LSV) in the range from 0.02 to 1.2 V at a sweep rate of 20 mV s⁻¹. The electrolyte was preliminarily saturated with oxygen for 60 min, the electrode being rotated at a speed of 700 rpm. The contribution of the ohmic voltage drop was considered according to the generally accepted method, as described in [35]. The contribution of the processes occurring at the electrode in the deoxygenated solution (Ar atmosphere) was taken into account [39]. LSVs were recorded at rotational speeds of the disk electrode of 400, 900, 1600, 2500 rpm. The activity of the catalysts in ORR (kinetic current) was determined from the normalized voltammograms with regard to the contribution of mass transfer when RDE was used [40, 41]. The calculation of the kinetic current at a potential of 0.90 V was carried out according to the Koutetsky-Levich, as described in [36].

The stability of the catalysts was assessed by stress testing methods based on multiple voltammetric cyclic potential changes at a rate of 100 mV s⁻¹ (a) for 5000 cycles in the potential range of 0.6–1.0 V and (b) for 1000 cycles in

the potential range of 0.6–1.4 V. Measurements were carried out in a 0.1 M HClO₄ solution saturated with argon at 25 °C. After every 500 (a) or 100 (b) cycles, two CVs were recorded in the potential range of 0.04–1.2 V at a potential sweep rate of 20 mV s⁻¹. The ESA was calculated using the second CV as described above. Stability was assessed by the absolute and relative change in the platinum ESA during and at the end of the stress test (ESA₅₀₀₀ and ESA₅₀₀₀/ESA₀). The catalysts ORR activity was also measured before and after stress testing.

For some catalysts, material degradation was also assessed by the method of superimposing rectangular potential pulses. In this case, the electrode was kept for 10,000 consecutive cycles at $E = 1.5$ V (3 s) and $E = 0.6$ V (3 s). Upon completion of stress testing, stability was assessed by changing ESA and catalyst activity in the ORR. The amount of electricity (Q_{kat} , Q_{an}) passed through the electrode under study was compared too.

3 Results and discussion

Pt-loading ($\omega(\text{Pt}\%)$) in the synthesized samples ranged from 20 to 23%wt. (Table 1), which is close to the value calculated from the precursor loading (23%wt.). Catalysts E1N and E2N based on C1N and N-doped graphene nanosheets, respectively, contain a larger fraction of the metal component than sample E1, which may be due to the stronger electronic interaction of the active centers of the support with NPs [40]. Thus, the presence of nitrogen atoms incorporated into the structure of the carbon support improves the adhesion of platinum nanoparticles to its surface.

The X-ray diffraction patterns of the samples are typical of Pt/C materials (Fig. S2). The broadening of the platinum characteristic reflections, which is especially pronounced for the E2N sample, is due to the small size of the crystallites. As a rule, for nanostructured Pt/C materials, a maximum of 111 is observed in diffractograms at values of 2 theta 39.9 degrees, as it is the case for JM and E1. However, for the E1N and E2N catalysts based on nitrogen-doped carriers, the position of the maximum corresponds to angles of 39.1 and 39.3 degrees 2 theta (Fig. S2). The shift of the reflection maximum toward smaller values of the 2 theta angles may be caused by the broadening of the platinum reflections and by the fitting peculiarity of wide peaks. This effect is opposite to the previously established effect of a decrease in the size of platinum NPs on the value of the crystal lattice parameter [43]. Doping of carbon with nitrogen also leads to a shift in the position of the maximum characteristic of carbon in the diffractogram toward larger angles (Fig. S2): the value of 2 theta of the “carbon” maximum increases in the series C1 < C1N < C2N from 24.2 to 25.2 degrees (Fig. S2) [44].

All the obtained Pt/C materials are characterized by a small platinum crystallite size - from about 0.8 to 1.3 nm (Table 1). Micrographs of different samples of platinum-carbon catalysts show certain features in the distribution of platinum nanoparticles, apparently due to the specific structure of the supports (Fig. S3). For the E1 material, there is an uneven distribution of nanoparticles on the surface and in the pores of the carrier, as well as the areas poorly filled with particles (Fig. S3a, Fig. 1a–c). The E1N material based on the nitrogen-doped C1N support is characterized by a more uniform distribution of platinum nanoparticles (Fig. 1d–f). In this case, a significant fraction of Pt nanoparticles is localized at the edge regions of the C1N support, forming circular paths of spatial distribution (Fig. S2b, Fig. 1d–f). According to [31], this may indicate the presence of mesopores, their edges being the places thermodynamically preferable for the sorption of platinum nanoparticles. Our data are consistent with [20]. In this work, it was shown that platinum nanoparticles, deposited during liquid-phase synthesis on N-doped Ketjenblack support, are distributed mainly on the surface of meso- and macropores, rather than in micropores, which afterward makes them available for reagents.

Note that the E2N catalyst differs significantly in its structure from the rest of the samples (Fig. 1g–i), which is due to the specific microstructure of the C2N support: nitrogen-doped graphene sheets do not contain pores. In this case one should note the high uniformity of the nanoparticles distribution on the surface of this support.

The average size of platinum nanoparticles, calculated from the TEM data (Fig. 1), increases in the series E1 < E2N ≤ E1N from 1.6 to 2.0 nm (Table 1). The sizes of NPs, determined by the TEM, and the average sizes of platinum crystallites, calculated from the XRD results, correlate with each other (Table 1). In the same series, the surface area of the support decreases (Table 1), which, apparently, determines the observed change in the NP size. Due to the high surface area of support C1, it can be assumed that on it the number of active sorption centers of the platinum nanoparticles (or centers of their growth in the case of a heterogeneous nucleation mechanism) is greater, as well as the average distance between the nanoparticles in the E1 catalyst. The E1 sample is also characterized by the narrowest distribution in the size of NPs (Fig. 1). The largest size of the nanoparticles in the E1N material is apparently due to the smallest surface area of this support. Nevertheless, all the obtained catalysts contain platinum nanoparticles, which are smaller than the commercial platinum-carbon reference JM (Table 1). Note that the value of the average size of Pt nanoparticles in a commercial sample calculated by the obtained TEM photographs is in good agreement with the literature data [45].

The surface and porosity of the C1 and C1N supports, as well as the E1 and E1N platinum-containing catalysts

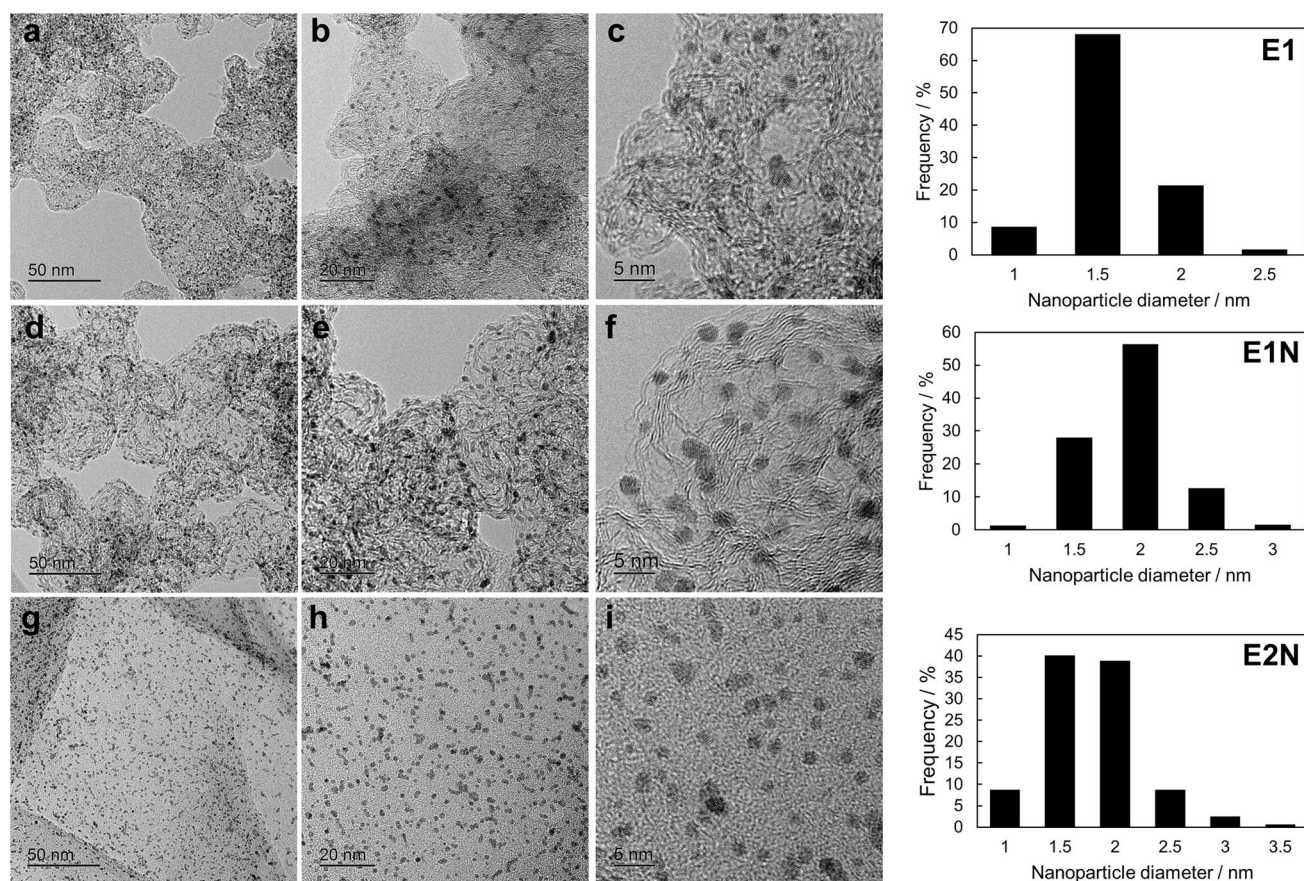


Fig. 1 Transmission electron microscopy photographs for materials E1 (a–c), E1N (d–f), and E2N (g–i) and histograms of the nanoparticle size distribution in the corresponding materials

Table 2 Surface area and porosity of carbon supports, and Pt/C materials based on them

Sample	Single point surface area at P/Po	BET surface area, $\text{m}^2 \text{g}^{-1}$	BJH Adsorption cumulative surface area of pores, $\text{m}^2 \text{g}^{-1}$	BJH desorption cumulative surface area of pores, $\text{m}^2 \text{g}^{-1}$	Pore volume $\text{cm}^3 \text{g}^{-1}$	Pore size, A		
						Adsorption average pore width (4 V/A by BET), A	BJH adsorption average pore diameter (4 V/A)	BJH desorption average pore diameter (4 V/A)
C1	1324	1352	3864	1225	2.03	60.2	11.3	38.7
E1	934	957	2775	907	1.35	59.5	11	35.7
C1N	343	345	884	338	0.71	82.8	13.8	39.4
E1N	370	378	1036	340	0.65	68.2	11.5	36.2

synthesized on their basis, were studied by the method of low-temperature nitrogen adsorption (Table 2; Fig. 2).

The isotherms shape of all samples could be attributed to Type IV, according to IUPAC notification [46]. It indicates a mesoporous adsorbent. Monolayer coverage completely forms at low relative pressure about 0.01, and multilayer adsorption begins at higher relative pressures (Fig. 2a, b) [47]. Hysteresis loop could be associated with capillary condensation of nitrogen in mesopores or the spaces between

particles. The shape of the hysteresis loop could be assigned to type H3 in IUPAC notification [46]. Porosity distribution was estimated by the original density functional theory according to the model of the slit pores on carbon. We have observed reduction of both micro and mesopores' volume after N-doping. Moving to Pt composites, pore-sized distribution of C1 and E1 samples exhibit the same shape with lower pore volume for E1 sample. It indicates that Pt nanoparticles on the surface of C1 substrate block part of micro

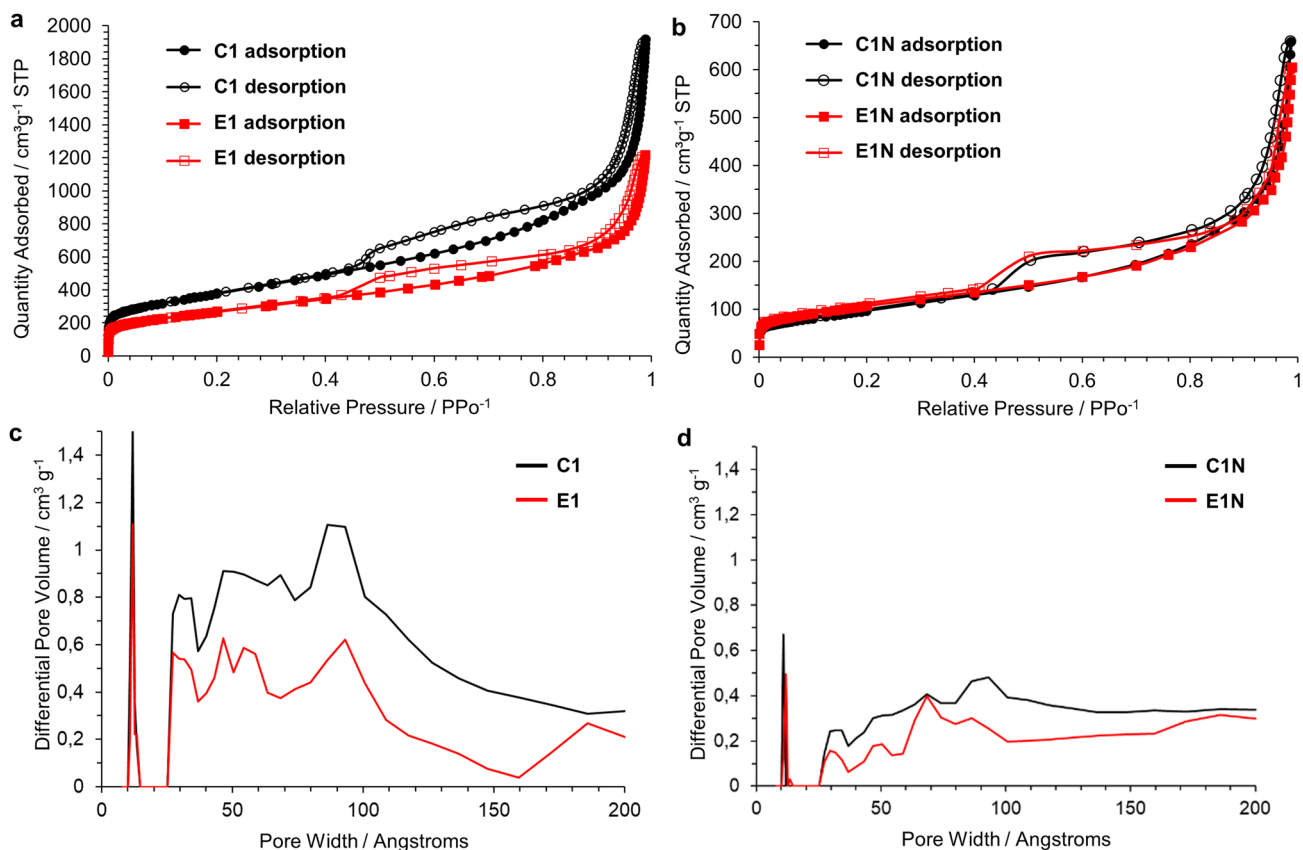


Fig. 2 N_2 adsorption–desorption isotherms of samples (a, b) and pore width distribution (c, d). Adsorption branches of isotherms contain filled markers, during desorption ones—empty markers

and mesopores. In the case of C1N and E1N samples, we have observed very close pore size distributions without significant reduction of pore volume. It could be associated with localization of Pt nanoparticles on the surface of carbon substrate rather than inside the pores.

The specific surface areas were estimated as 1352, 957, and 345, 378 $m^2 g^{-1}$, according to the BET model for the samples C1, E1, and C1N, E1N, respectively. In all cases, correlation coefficients were higher than 0.9997 (Fig. S4). Pore volumes exhibited the same trend as BET specific surface areas (Table 2). The highest pore volume of 2.03 $cm^3 g^{-1}$ was observed for the sample C1. The E1 catalyst based on this support is characterized by a decrease in the pore volume to 1.35 $cm^3 g^{-1}$, apparently due to their partial isolation by platinum nanoparticles, which fill the pores during the chemical synthesis.

It is known that in the process of N-doping of carbon supports, doped pyrocarbon is deposited mainly in micropores, thus making impossible the subsequent deposition of platinum nanoparticles in them. Such materials are mainly characterized by the presence of mesopores [30, 31]. When studying the C1N support by the XPS method, it was found [30] that N-doped pyrocarbon was uniformly distributed

over the support surface. A significant decrease (by a factor of 4) in the surface area and pore volume of the C1N material compared to the initial C1 (Table 2; Fig. 2c, d), which was observed as a result of chemical modification, indicates that the pores of the support are largely filled with N-doped pyrocarbon, as noted in [29]. This is confirmed by a comparison of the size distribution of pores in materials C1 and C1N (Fig. 2c, d).

An insignificant change in the surface area in terms of BET, observed upon passing from an N-doped C1N support (345 $m^2 g^{-1}$) to a platinum-containing material E1N based on it (378.4 $m^2 g^{-1}$), may be due to the primary distribution of platinum nanoparticles on the surface of the carrier along the perimeter and beyond the perimeter of the mesopores, which does not result in the pores isolation and a decrease in the surface area (Table 2; Fig. 2c, d). Apparently, it is energetically favorable for platinum nanoparticles to be fixed on such a surface due to the interaction with nitrogen-containing centers.

According to the XPS studies, the concentration of the surface oxygen atoms in samples E1 and JM on an unmodified carbon support is 11.8 and 11.0 %, respectively, (Fig. S5, Table S1). For the E1N sample, the XPS results confirm

Table 3 Some parameters characterizing the electrochemical behavior of Pt/C catalysts

Sample	ESA H _{ads} /H _{des} , m ² g ⁻¹ (Pt)	ESA CO _{ads} , m ² g ⁻¹ (Pt)	Half-wave potential of O ₂ reduction, E _{1/2} , V	ORR kinetic currents at E=0.90 V		
				I _k , mA	I _k , A g ⁻¹ (Pt)	I _k , A m ⁻² (Pt)
E1	114	120	0.87	0.39	56	0.50
E1N	110	115	0.91	1.72	244	1.75
E2N	118	130	0.85	0.60	81	0.70
JM	84	78	0.91	1.33	184	2.19

the presence of nitrogen, as well as a reduced oxygen content in the composition as compared to other samples.

Analysis of N1s XPS spectra (Fig. S5b) shows that nitrogen is mostly in the pyridine (Table S2 A), imine (C=N-H) and/or pyridone (C-N=O) forms (Table S2 C) and in the so-called quaternary (N⁺-H) groups (Table S2 D) in E1N sample (Fig. 5b, Table S2) [48, 49].

Figure S5c shows the Pt4f7/2,5/2 spectra of the E1N sample. Table S3 shows the binding energies and the relative contents of the Pt4f7/2 components of the spectra for all the studied samples. The binding energies of Pt4f7/2 spectra correspond to the metallic state of the platinum atoms (components A), and to the oxidized forms PtO (component D) and PtO₂ (component E). Note, the E1N sample is characterized by the absence of the E component, and a higher proportion of the D component, in comparison with other investigated materials. This feature of the E1N catalyst composition may be due to the effect of nitrogen-doped support on the platinum nanoparticles reactivity with respect to oxygen.

Before discussing the features of the catalysts electrochemical behavior, it should be noted that there are noticeable differences in their hydrophilicity, which can affect the structure of the catalytic layer formed at the end of the glassy carbon disk (see the Experimental Technique section). Catalytic inks containing E2N, E1 and JM were applied to the RDE end, with a uniform drop (layer) being formed. In contrast to them, when applying the N-doped E1N material, a less uniform distribution of ink on the RDE, the dripping, the formation of the so-called coffee ring [21] were observed when the applied layer dried. Such effects may be due to a change in the hydrophobicity of the support during its modification [31, 50].

Preliminary cycling of the carbon carriers (Fig. S6a) showed the presence of pseudocapacitance peaks localized on CV at 0.45 V and associated with the presence of oxygen-containing groups on the carbon surface. At the same time, the magnitude of the current in the double-layer region of CV correlates with the area of the electrochemically accessible carbon surface. Judging by the intensity of the peaks near the potential of 0.45 V, the C1 carrier has a more oxidized surface compared to the

two modified carriers (Fig. S6a). This is consistent with the literature data, according to which unmodified carbon supports are often characterized by the presence of many oxygen-containing groups on the surface [21, 50].

Cyclic voltammograms recorded during the electrochemical activation (standardization) of the surface of platinum-containing catalysts are shown in Figure S7. The largest number of potential sweep cycles was required to activate the E1N surface, while the stabilization of the current values on the CVs of the E1, JM, and especially E2N catalysts occurred faster. Apparently, the hydrophobicity of E1N slows down the access of the electrolyte to all platinum nanoparticles located in the catalytic layer. In the process of activation, its surface is hydrophilized.

Cyclic voltammograms of activated samples have a form typical for Pt/C catalysts (Fig. 3a). The currents in the double-layer region, corresponding to the charge/discharge processes of the electric double-layer, increase in the series JM < E1N < E2N < E1, which is due to an increase in the surface area of carbon carriers in this series (Table 2). At the same time, the values of the electrochemically active surface area of platinum (ESA) are close in all the catalysts that we have obtained and significantly exceed the ESA of the commercial reference sample JM (Table 3). They decrease in the series: E2N ≥ E1 ≥ E1N >> JM. The high (110–130 m² g⁻¹ (Pt)) ESA values of the obtained samples are largely caused by the specific character of the synthesis method [50], which makes it possible to obtain the nanoparticles which are much smaller than those in the commercial JM sample (Table 3). The catalysts ESA values calculated by electrochemical adsorption/desorption of atomic hydrogen (Fig. 3a) and by oxidation of CO chemisorbed monolayer (Fig. 3b), correlate well with each other (Table 3). Note that the oxidation onset potential of chemisorbed CO on the E1N catalyst is approximately 40 mV higher than that of the other studied samples, and the range of potentials corresponding to the current maximum is broadened (inset in Fig. 3b).

The catalysts activity in ORR was estimated by the values of kinetic currents, calculated by the Koutetsky-Levich equation and the potentials of the oxygen half-wave (Table 3; Fig. 3). Despite the high ESA and small size of the platinum nanoparticles, the E2N material is characterized by a specific

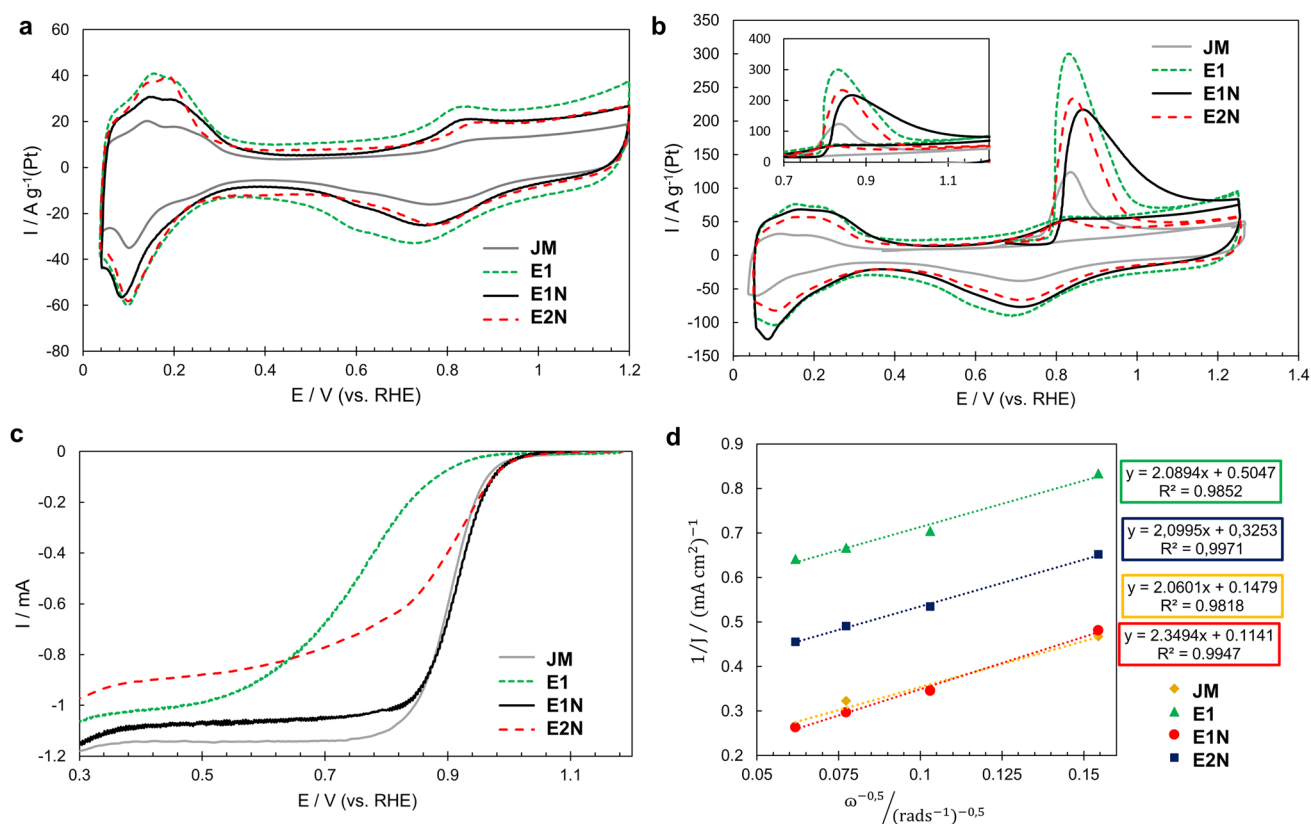


Fig. 3 Cyclic voltammograms of Pt/C electrodes: **a** after surface standardization; **b** after CO transmission. Electrolyte is 0.1 M HClO_4 , atmosphere consists of Ar. The sweep rate is 20 mV s^{-1} . **c** Linear voltammograms of the ORR. The rotation speed of the disk is 1600 rpm;

volt-ampere curve and low specific currents (Fig. 3c). The reason for the unexpectedly low specific activity of this sample may be the problems caused by mass transfer of oxygen to the platinum surface arising in the layer of the supported catalyst. Apparently, carbon “nanosheets” overlap with each other, which makes it difficult to diffuse oxygen molecules to platinum nanoparticles located between the sheets and/or in the depth of the catalytic layer. The unusual character of mass transfer is reflected in the shape of the voltammogram, which, for this material, possesses a slope not typical for the diffusion-kinetic region (Fig. 3c). Problems of the reagent mass transfer can also determine the low ORR activity of the E1 catalyst (Fig. 3; Table 3). The point is that the high surface area of the KetjenBlack EC DJ-600 carrier is due to the presence of a large number of micropores [50]. The deposition of platinum NPs in such pores during the Pt/C synthesis creates a problem with the oxygen access to their surface during the catalyst operation.

The values of the kinetic ORR current increase in the series $\text{E1} < \text{E2N} < \text{JM} < \text{E1N}$. Significantly higher activity of E1N compared to E1, in principle, can be associated both with the optimal placement of Pt NPs, as there are no

d $1/j - \omega^{-0.5}$ dependence at 0.90 V potential. The rate of the potential sweep is 20 mV s^{-1} , 0.1 M HClO_4 solution-saturated O_2 at atmospheric pressure

micropores in the support, and with the positive effect of the nitrogen atoms on the spatial distribution and the platinum NPs activity in ORR. Since the value of the specific platinum activity ($\text{A m}^{-2}(\text{Pt})$) in the E1N catalyst is lower than in JM (Table 3), we believe that the optimization of the carbon (KetjenBlack EC DJ-600) structure becomes the main factor of influence because of its N-doping. Note that the small size of platinum NPs can also have a negative effect on the specific activity of this catalyst [51]. Nevertheless, the combination of a rather high specific activity in ORR and the highest ESA cause maximum mass activity of the E1N catalyst, exceeding the one for JM (Table 3).

The catalysts durability was initially estimated by the methods of multiple voltammetric cycles in two potential ranges of 0.6–1.0 V and 0.6–1.4 V for 5000 and 1000 cycles, respectively¹. It is known that under the conditions of “mild” stress testing (with a potential sweep up to 1.0 V), the main

¹ A corrosion resistance assessment of the carbon carriers in the “start-stop” stress testing mode and a discussion of the results obtained are given in Supplementary Information (Fig. S4b, c).

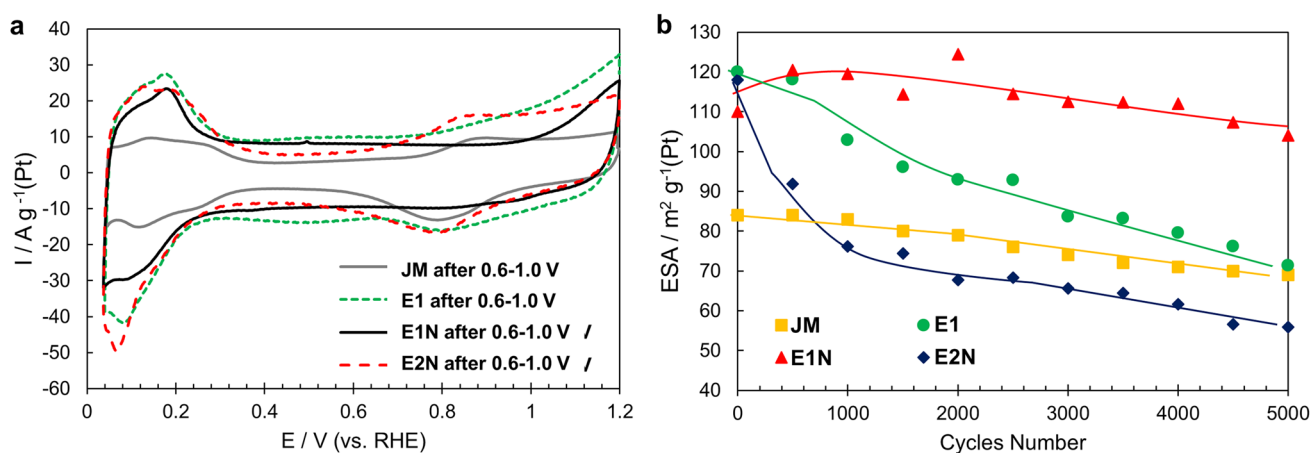


Fig. 4 **a** Cyclic voltammograms of Pt/C electrodes after stress test. Electrolyte is 0.1 M HClO₄, Ar atmosphere. The sweep rate is 20 mV s⁻¹. The potentials range is 0.6–1.0 V, 23 °C. **b** Change ESA of Pt/C materials during stress testing

contribution to the degradation of the catalyst is made by the processes associated with the dissolution, aggregation, and Ostwald ripening of Pt nanoparticles [51, 52]. Analysis of the ESA dependence on the number of stress test cycles (Fig. 4a) showed that in this test mode, E2N and E1 catalysts degrade faster. A significant current decrease in the hydrogen region of the CV associated with a decrease in ESA of E2N and E1 materials during the stress test is shown in Fig. S8. The ESA of the commercial JM catalyst decreases more slowly. The ESA value of the E1N material increases during the first 1500–2000 cycles and only then slightly decreases (Fig. 4a). Note that after the completion of stress testing, the characteristic regions in the oxygen part of the CV, observed for Pt/C catalysts, are also most pronounced for the E1N catalyst (Fig. 4b).

The established features of the catalyst degradation are reflected in the change in their ORR activity. Figure 5 shows the oxygen reduction voltammograms measured on the respective catalysts before and after the stress test. The lowest shift of the volt-ampere curves to the region of lower potentials, which is characteristic of the samples that passed the stress test, is observed for the E1N and JM catalysts, and the highest one - for the E2N catalyst. This means that the decrease in the catalysts ORR activity, which is the result of the stress test, intensifies in the same series in which the ESA drop increases: E1N ≤ JM < E1 < E2N. The corresponding values of ESA, ORR activity, and oxygen half-wave potentials of the catalysts after the stress test are shown in Table 4.

Potential cycling in the 0.6–1.4 V range has a much more aggressive effect on Pt/C catalysts than stress testing in the “soft” (0.6–1.0 V) mode. For all catalysts, during the stress test, there is a decrease in currents in the hydrogen region of the CVs (Fig. S9), a decrease in the ESA values and the ORR activity (Table 4; Figs. 6 and 7).

During the cycling of the E1 catalyst, a significant broadening of the double-layer CV region also occurs, indirectly indicating the degradation of the C1 support, which has the highest surface area (Fig. 6a). Broadening of the CV in the double-layer region for support C1, was also noticed in the corrosion resistance study of the carbon supports (Fig. S6a, c). Comparison of the investigated catalysts characteristics showed that the E1N catalyst also exhibited the highest stability under the conditions of a “hard” stress test. Thus, its ESA decreased from 110 to 40 m² g⁻¹(Pt), and its specific activity from 1.75 to 1.0 A m⁻²(Pt), while for the commercial JM catalyst ESA decreased from 84 to 24 m² g⁻¹(Pt), and the specific activity fell from 2.19 to 0.8 A m⁻²(Pt) (Tables 3 and 4).

Analysis of the catalysts behavior during stress testing in different modes, as well as comparison of the initial and final (at the end of stress tests) values corresponding to ESA and ORR activity (Table 4; Figs. 4 and 6) indicate the highest stability of the E1N sample. Figure 8 graphically shows the relationship degree of degradation and changes ESA (stability) during various stress tests for all materials. As a rule, the stability of Pt/C catalysts under the conditions of the “soft” testing regime increases with an increase in the average NP size and the Pt-loading in the catalyst [52–54]; however, a E1N sample containing nanoparticles with an average size of about 2.0 nm has demonstrated higher stability than the commercial JM sample, containing particles of about 2.8 nm. Apparently, the doping of carbon with nitrogen enhances the adhesion of platinum NPs to the support, which prevents the detachment or movement of particles over the surface of the support and their aggregation during the stress test. The porous structure of the carriers also plays an important role in terms of resistance to degradation. Thus, despite the doping with nitrogen, the E2N catalyst based on the atomically smooth and non-porous support

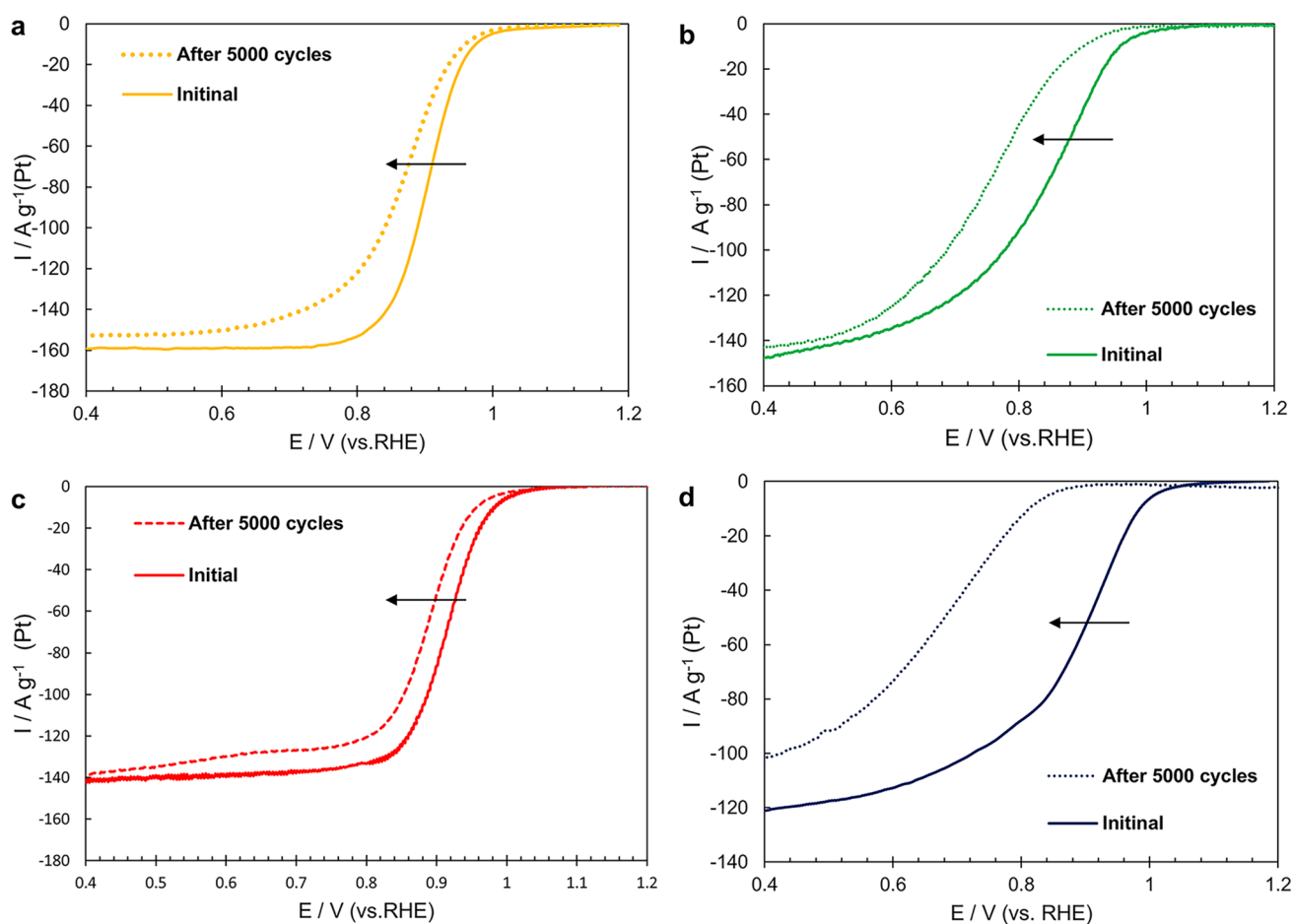


Fig. 5 Linear voltammograms of the ORR for the catalysts before and after stress test **a** JM; **b** E1; **c** E1N; **d** E2N. The rotation speed of the disk is 1600 rpm

Table 4 Some parameters characterizing the electrochemical behavior of catalysts after the completion of stress testing

Sample	5000 cycles at 0.6–1.0 V		ORR activity of catalysts at $E=0.90$ V	
	ESA ₅₀₀₀ , m ² g ⁻¹ (Pt)	$E_{1/2}$, V	I_k , A g ⁻¹ (Pt)	I_k , A m ⁻² (Pt)
E1	66	0.76	12	0.30
E1N	101	0.89	88	0.90
E2N	50	0.78	2	0.10
JM	69	0.88	60	0.87
Sample	1000 cycles at 0.6–1.4 V			
	ESA ₁₀₀₀ , m ² g ⁻¹ (Pt)	$E_{1/2}$, V	I_k , A g ⁻¹ (Pt)	I_k , A m ⁻² (Pt)
E1	22	0.72	5	0.18
E1N	40	0.88	54	1.00
E2N	18	0.67	1	0.03
JM	24	0.86	41	0.80

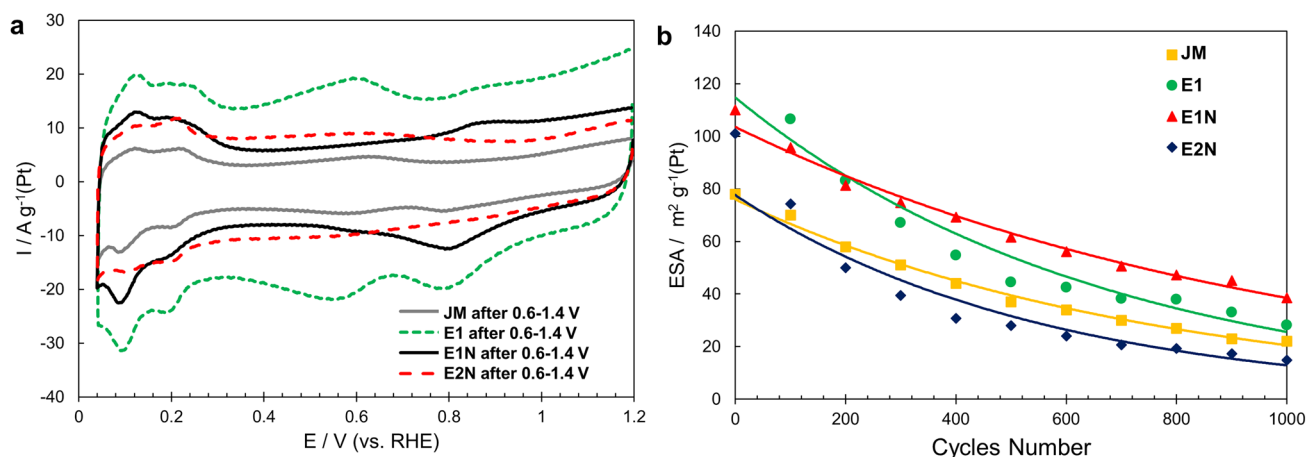


Fig. 6 **a** Cyclic voltammograms of Pt/C electrodes after stress test. Electrolyte is 0.1 M HClO₄, Ar atmosphere. The sweep rate is 20 mV s⁻¹. **b** Change ESA of Pt/C materials during stress testing. The range of potentials is 0.6–1.4 V. 23 °C

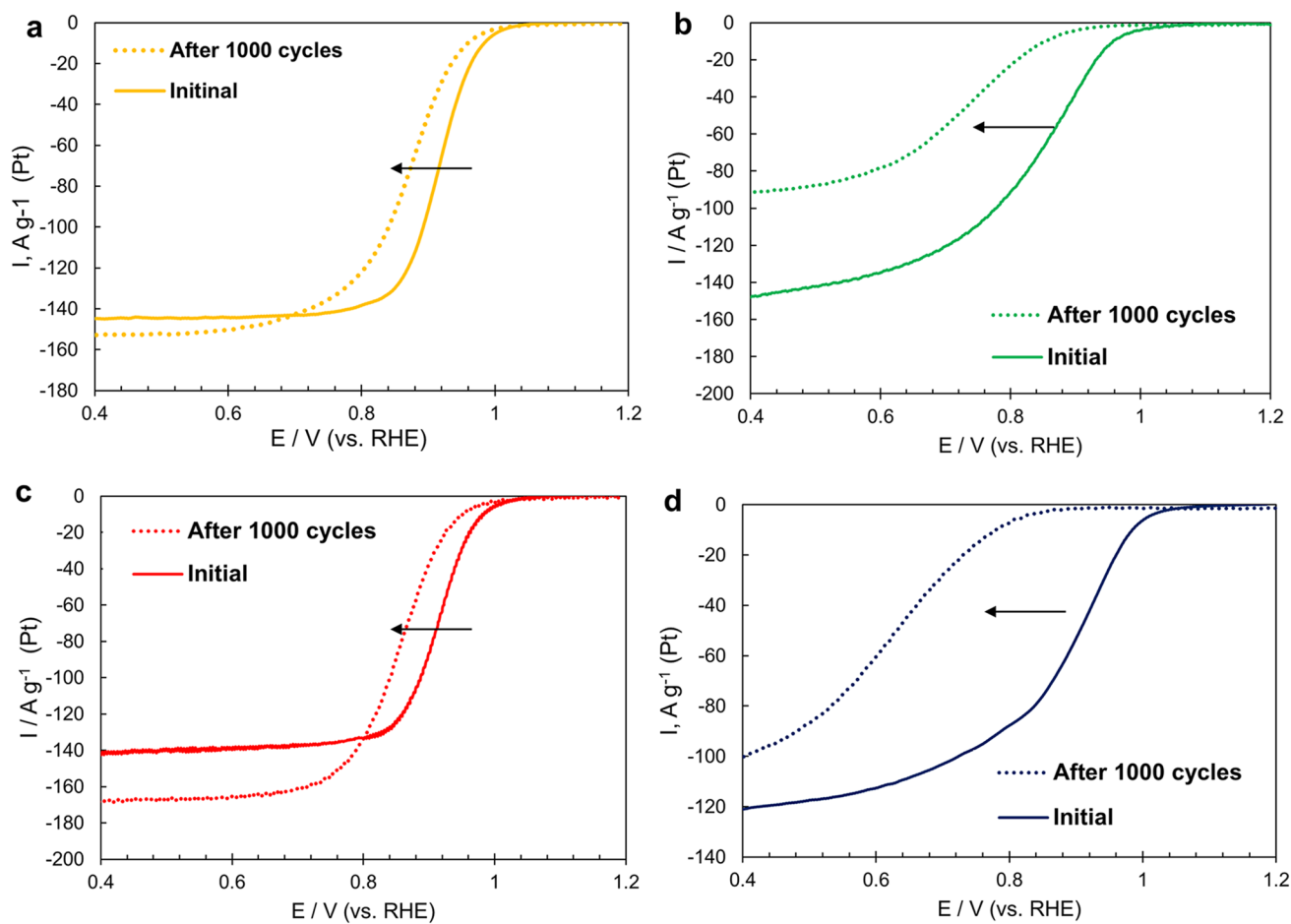


Fig. 7 Linear voltammograms of the ORR initial and after stress test 0.6–1.4 V, 1000 cycles. The rotation speed of the disk is 1600 rpm; **a** JM; **b** E1; **c** E1N; and **d** E2N

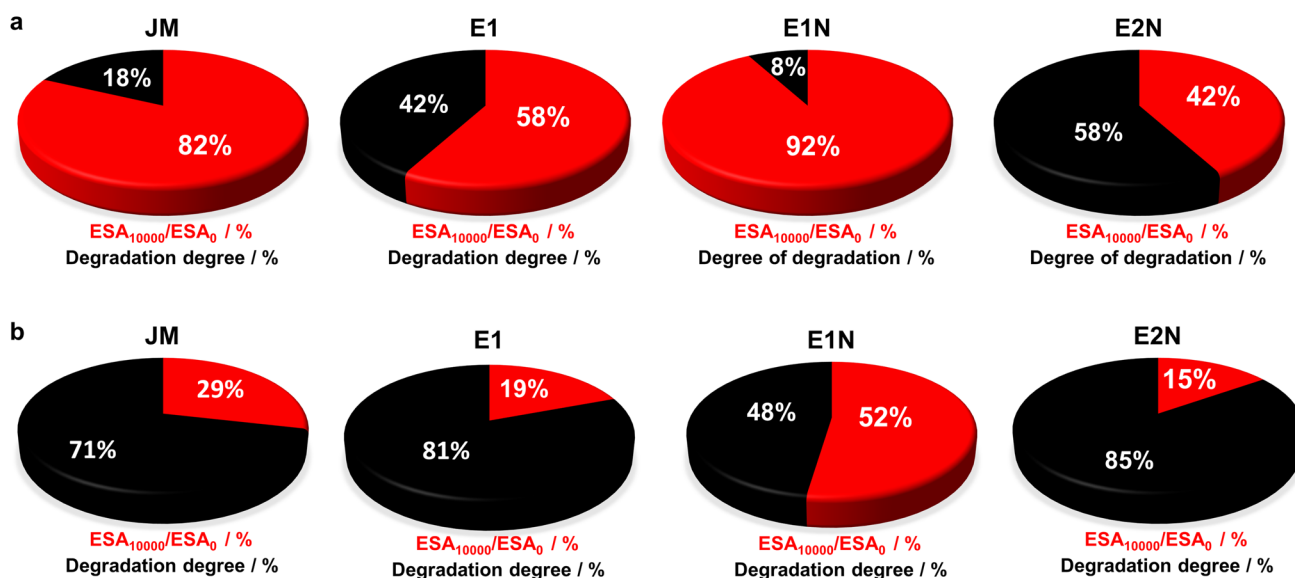


Fig. 8 ESA loss (%) and degradation degree for Pt/C catalysts in different stress tests. **a** 0.6–1.0 V, 5000 cycles; **b** 0.6–1.4 V, 1000 cycles

apparently is not able to effectively resist the aggregation of platinum nanoparticles, which results in a rapid decrease in both ESA and mass activity during stress testing (Figs. 4, 5 and 6; Table 4).

In our opinion, the main problem with the voltammetric aspect of the stress testing methods is the comparison of the degradation degree in different catalysts, which is made without the amounts of substances that have reacted on the electrodes during testing, being taken into account. Therefore, for the two catalysts that showed the highest stability, we tried to determine the degree of degradation combined with the measurement of the charge consumed in the Faraday processes. To this end, the stabilities of E1N and commercial JM electrocatalyst were studied in the “start-stop” testing mode, which consisted of multiple (10,000 cycles)

superposition of three-second rectangular potential pulses at 0.6 and 1.5 V. The stability of the catalysts was assessed by the change in the ESA. We assumed that the greater the amount of charge passed through the electrode during the stress test, the more active catalyst of the corresponding Faraday processes it was. In this case, the cathode (at a potential of 0.6 V) and anode (at a potential of 1.5 V) amounts of charge were summed up separately. The results of the stress test performed are shown in Fig. 9. And in this case, the E1N catalyst obtained on a doped support had the highest residual electrochemically active surface area of $40 \text{ m}^2 \text{ g}^{-1}(\text{Pt})$, while the ESA of the commercial analog JM after the stress test decreased to $24 \text{ m}^2 \text{ g}^{-1}(\text{Pt})$. During the stress test, mainly for the Faraday processes on the E1N catalyst, approximately 2

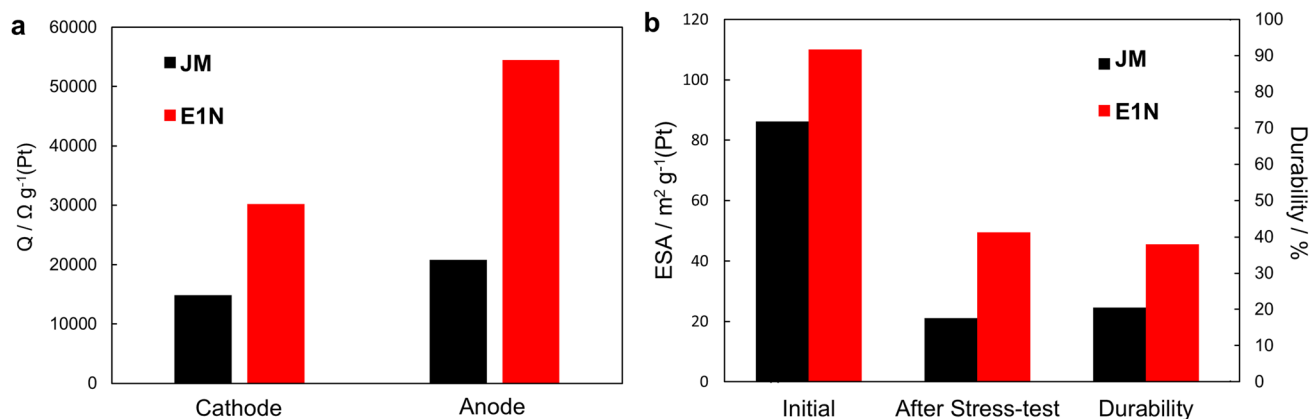


Fig. 9 **a** The amount of charge passed during stress testing (Q); **b** Values of initial and residual (after stress test) ESA, and relative durability of electrocatalysts

times more cathode and approximately 2.5 times more anode amounts of charge were consumed, than on the JM catalyst.

4 Conclusions

Platinum-carbon catalysts containing from 20 to 23%wt. platinum were obtained by a liquid-phase formaldehyde synthesis. Carbon C1 (Ketjenblack EC 600-jD, surface area about $1400 \text{ m}^2 \text{ g}^{-1}$) and nitrogen-doped carbon materials C1N and C2N were used as carriers. The nitrogen-containing support C1N obtained from Ketjenblack EC 600-jD had a surface area of about $345 \text{ m}^2 \text{ g}^{-1}$, while the non-porous support C2N, consisting of atomically smooth graphene sheets modified with nitrogen, had a surface area of about $270 \text{ m}^2 \text{ g}^{-1}$. The average size of platinum nanoparticles in the obtained catalysts, increasing in the series $E1 < E2N < E1N$, ranged from 1.5 to 2 nm. As a result, their ESA ($110\text{--}130 \text{ m}^2 \text{ g}^{-1}(\text{Pt})$) was significantly higher than that of the commercial JM analog (Hispec3000) ($84 \text{ m}^2 \text{ g}^{-1}(\text{Pt})$). The presence of nitrogen atoms in the graphene layers of carbon supports had led to an increase in their sorption capacity with respect to platinum NPs; therefore, the deposition of platinum on C1N and C2N during the synthesis of catalysts occurred almost quantitatively.

The electrochemical behavior of the obtained catalysts is determined by the features of the shape and structure of the support particles, the placement of platinum nanoparticles on the surface and in the pores of carbon materials, the adhesion strength of the nanoparticles to the support, and also their size and size distribution of the nanoparticles, which determine the catalysts ESA value. The specific activity of catalysts in ORR turned out to be the highest for E1N and JM samples, while in the process of oxygen electroreduction in the deposited layers of E1 and E2N catalysts, there arises the problem with the reagent delivery to the platinum nanoparticles located deep in the layer. We believe that this is due to the placement of a significant part of NPs in the micropores of the E1 catalyst and the overlap of diffusion flows by separate sheets of the support (E2N). The mass activity of catalysts in ORR increases in the series $E1 < E2N < JM < E1N$. At the same time, the specific activity of the E1N catalyst is lower than that of the JM, which means that the key factor responsible for its high mass activity is precisely the high ESA.

The catalysts stability, determined by changes in the ESA and ORR activity in three different stress testing modes, increases in the following order: $E2N < E1 < JM < E1N$. The maximum stability of the E1N sample is apparently due to a combination of the optimal structure (porosity and placement peculiarities of platinum nanoparticles in pores) and the positive effect of nitrogen

atoms intercalated into carbon on the adhesion strength of platinum nanoparticles to the support. Note that, according to the results of study performed on the porosity of materials by the method of low-temperature nitrogen adsorption, the deposition of platinum NPs on the C1N support practically did not result in pore closure. The amount of electricity consumed for the Faraday reactions during the “start-stop” stress test (multiple superposition of potential pulses at 0.6 and 1.5 V) on the E1N catalyst significantly exceeds that for the commercial JM sample.

Thus, the E1N catalyst synthesized with nitrogen-doped carbon showed a markedly higher ORR activity and durability compared not only to other synthesized materials, but also to the commercial JM catalyst. Taking into account that the doping of carriers with nitrogen improves the interaction of the catalytic layer with the ionomer [3, 20], one can assume that such a catalyst will be even more efficient in the membrane-electrode assembly. We are planning to check this in our further research. We also believe that the nitrogen-doped C1N support could be a very promising material in producing two-component PtM catalysts.

The research is the original one and has not been published before.

Supplementary Information The online version contains supplementary material available at <https://doi.org/10.1007/s10800-021-01629-y>.

Acknowledgements The authors are grateful to Dr. Kozakov A.T. and Dr. Nikolsky A.V. for conducting the XPS study and to Mr. Nikulin A.Yu. for conducting the XRD study. This research was financially supported by the Ministry of Science and Higher Education of the Russian Federation (State assignment in the field of scientific activity No 0852-2020-0019).

References


1. Khodabakhshi S, Fulvio PF, Andreoli E (2020) Carbon black reborn: structure and chemistry for renewable energy harnessing. *Carbon* 162:604–649. <https://doi.org/10.1016/j.carbon.2020.02.058>
2. Dicks AL (2006) The role of carbon in fuel cells. *J Power Sources* 156:128–141. <https://doi.org/10.1016/j.jpowsour.2006.02.054>
3. Ramaswamy N, Gu W, Ziegelbauer JM, Kumaraguru S (2020) Carbon support microstructure impact on high current density transport resistances in PEMFC cathode. *Electrochem Soc* 167:064515. <https://doi.org/10.1149/1945-7111/ab819c>
4. Antolini E (2009) Carbon supports for low-temperature fuel cell catalysts. *Appl Catal B: Environ* 88:1–24. <https://doi.org/10.1016/j.apcatb.2008.09.030>
5. Wang Y-J, Fang B, Li H, Bi XT, Wang H (2016) Progress in modified carbon support materials for Pt and Pt-alloy cathode catalysts in polymer electrolyte membrane fuel cells. *Prog Mater Sci* 82:445–498. <https://doi.org/10.1016/j.pmatsci.2016.06.002>
6. Sharma R, Andersen SM (2018) An opinion on catalyst degradation mechanisms during catalyst support focused accelerated stress test (AST) for proton exchange membrane fuel cells

- (PEMFCs). *Appl Catal B* 239:636–643. <https://doi.org/10.1016/j.apcatb.2018.08.045>
7. Eguizabal A, Uson L, Sebastian V, Hueso JL, Pina MP (2015) Efficient and facile tuning of Vulcan XC72 with ultra-small Pt nanoparticles for electrocatalytic applications. *RSC Advances* 5:90691–90697. <https://doi.org/10.1039/c5ra16698e>
 8. Macauley N, Papadiaz DD, Fairweather J, Spornjak D, Langlois D, Ahluwalia R, More KL, Mukundan R, Borup RL (2018) Carbon corrosion in PEM fuel cells and the development of accelerated stress tests. *J Electrochem Soc* 165:F3148. <https://doi.org/10.1149/2.0061806jes>
 9. Hussain S, Erikson H, Kongi N, Merisalu M, Ritslaid P, Sammelselg V, Tammeveski K (2017) Heat-treatment effects on the ORR activity of Pt nanoparticles deposited on multi-walled carbon nanotubes using magnetron sputtering technique. *Int J Hydrogen Energy* 42:5958–5970. <https://doi.org/10.1016/j.ijhydene.2016.11.164>
 10. Zhang W, Sherrell P, Minett AI, Razal JM, Chen J (2010) Carbon nanotube architectures as catalyst supports for proton exchange membrane fuel cells. *Energy Environ Sci* 3:1286–1293. <https://doi.org/10.1039/C0EE00139B>
 11. Cheng N, Mu S, Chen X, Lv H, Pan M, Edwards PP (2011) Enhanced life of proton exchange membrane fuel cell catalysts using perfluorosulfonic acid stabilized carbon support. *Electrochim Acta* 56:2154–2159. <https://doi.org/10.1016/j.electacta.2010.11.075>
 12. Hodnik N, Dehm G, Mayrhofer KJJ (2016) Importance and challenges of electrochemical in situ liquid cell electron microscopy for energy conversion research. *Acc Chem Res* 49:2015–2022. <https://doi.org/10.1021/acs.accounts.6b00330>
 13. Maillard F, Silva WO, Castanheira L, Dubau L, Lima FHB (2019) Carbon corrosion in proton-exchange membrane fuel cells: spectrometric evidence for Pt-catalysed decarboxylation at anode-relevant potentials. *ChemPhysChem* 20:3106–3111. <https://doi.org/10.1002/cphc.201900505>
 14. Wang XX, Tan ZH, Zeng M, Wang JN (2014) Carbon nanocages: a new support material for Pt catalyst with remarkably high durability. *Sci Rep* 4:4437. <https://doi.org/10.1038/srep04437>
 15. Schonvogel D, Hülstede J, Wagner P, Kruusenberg I, Tammeveski K, Dyck A, Agert C, Wark M (2017) Stability of Pt nanoparticles on alternative carbon supports for oxygen reduction reaction. *J Electrochem Soc* 164:F995. <https://doi.org/10.1149/2.1611709jes>
 16. Nunes M, Fernandes DM, Morales MV, Ramos R, GuerreroRuiz A, Freire C (2018) Cu-based N-doped/undoped graphene nanocomposites as electrocatalysts for the oxygen reduction. *J Appl Electrochem* 49:693–703. <https://doi.org/10.1007/s10800-019-01317-y>
 17. Stoller MD, Park S, Zhu Y, An J, Ruoff RS (2008) Graphene-based ultracapacitors. *Nano Lett* 8:3498–3502. <https://doi.org/10.1021/nl802558y>
 18. Cheng J, Li Y, Huan Xg, Wang Q, Meib A, Shen PK (2015) Highly stable electrocatalysts supported on nitrogen-self-doped three-dimensional graphene-like networks with hierarchical porous structures. *J Mater Chem A* 3:1492–1497. <https://doi.org/10.1039/c4ta05552g>
 19. Chen M, Hwang S, Li J, Karakalos S, Chen K, He Y, Mukherje S, Su D, Wu G (2018) Pt alloy nanoparticles decorated on large-size nitrogen-doped graphene tubes for highly stable oxygen-reduction catalysts. *Nanoscale* 10:17318–17326. <https://doi.org/10.1039/c8nr05888a>
 20. Harzer GS, Orfanidi A, El-Sayed H, Madkikar P, Gasteiger HA (2018) Tailoring catalyst morphology towards high performance for low Pt loaded PEMFC cathodes. *J Electrochem Soc* 165:F770. <https://doi.org/10.1149/2.0311810jes>
 21. Schmies H, Hornberger E, Anke B, Jurzinsky T, Nong HN, Dionigi F, Kühl S, Drnec J, Lerch M, Cremers C, Strasser P (2018) Impact of carbon support functionalization on the electrochemical stability of Pt fuel cell catalysts. *Chem Mater* 30:7287–7295. <https://doi.org/10.1021/acs.chemmater.8b03612>
 22. Cao J, Chu Y, Tan X (2014) Pt/XC-72 catalysts coated with nitrogen-doped carbon (Pt/XC-72@C-N) for methanol electro-oxidation. *Mater Chem Phys* 144:17–24. <https://doi.org/10.1016/j.matchemphys.2013.12.001>
 23. Davydova ES, Tarasevich MR (2016) Studies of selectivity of oxygen reduction reaction in acidic electrolyte on electrodes modified by products of pyrolysis of polyacrylonitrile and metalloporphyrins. *Russ J Electrochem* 52:1007–1014. <https://doi.org/10.1134/S1023193516110021>
 24. Jafri RI, Rajalakshmi N, Ramaprabhu S (2010) Nitrogen doped graphene nanoplatelets as catalyst support for oxygen reduction reaction in proton exchange membrane fuel cell. *J Mater Chem* 20:7114–7117. <https://doi.org/10.1039/c0jm00467g>
 25. Zhang L, Xia Z (2011) Mechanisms of Oxygen Reduction Reaction on Nitrogen-Doped Graphene for Fuel Cells. *J Phys Chem C* 115:11170–11176. <https://doi.org/10.1021/jp201991j>
 26. Mardle P, Ji X, Wu J, Guan S, Dong H, Du S (2020) Thin film electrodes from Pt nanorods supported on aligned N-CNTs for proton exchange membrane fuel cells. *Appl Catal* 260:118031. <https://doi.org/10.1016/j.apcatb.2019.118031>
 27. Zheng X, Wu J, Cao X, Abbott J, Jin C, Wang H, Strasser P, Yang R, Chen X, Wu G (2019) N-, P-, and S-doped graphene-like carbon catalysts derived from onium salts with enhanced oxygen chemisorption for Zn-air battery cathodes. *Appl Catal B* 241:442–451. <https://doi.org/10.1016/j.apcatb.2018.09.054>
 28. Gribov EN, Kuznetsov AN, Voropaev IN, Golovin VA, Simonov PA, Romanenko AV, Okunev AG (2016) Analysis of the corrosion kinetic of Pt/C catalysts prepared on different carbon supports under the “start-stop.” *Cycl Electrochem* 74:159–173. <https://doi.org/10.1007/s12678-015-0294-6>
 29. Golovin VA, Gribov EN, Simonov PA, Okunev AG, Voropaev IN, Kuznetsov AN, Romanenko AV (2015) Development of carbon supports with increased corrosion resistance for Pt/C catalysts for oxygen electroreduction. *Kinet Catal* 56:509–514. <https://doi.org/10.1134/S0023158415040072>
 30. Golovin VA, Maltseva NV, Gribov EN, Okunev AG (2017) New nitrogen-containing carbon supports with improved corrosion resistance for proton exchange membrane fuel cells. *Int J Hydrogen Energy* 42:11159–11165. <https://doi.org/10.1016/j.ijhydene.2017.02.117>
 31. Ott S, Orfanidi A, Schmies H, Anke B, Nong HN, Hubner J, Gernert U, Glied M, Lerch M, Strasser P (2020) Ionomer distribution control in porous carbon-supported catalyst layers for high-power and low Pt-loaded proton exchange membrane fuel cells. *Nat Mat* 19:77–85. <https://doi.org/10.1038/s41563-019-0487-0>
 32. Heydari A, Gharibi H (2016) Fabrication of electrocatalyst based on nitrogen doped graphene as highly efficient and durable support for using in polymer electrolyte fuel cell. *J Power Sources* 325:808–815. <https://doi.org/10.1016/j.jpowsour.2016.06.039>
 33. Ma JH, Wang L, Mu X, Li L (2015) Nitrogen-doped graphene supported Pt nanoparticles with enhanced performance for methanol oxidation. *Int J Hydrogen Energy* 40:2641–2647. <https://doi.org/10.1016/j.ijhydene.2014.12.080>
 34. Lin Z, Waller GH, Liu Y, Liu M, Wong CP (2013) Simple preparation of nanoporous few-layer nitrogen-doped graphene for use as an efficient electrocatalyst for oxygen reduction and oxygen evolution reactions. *Carbon* 53:130–136. <https://doi.org/10.1016/j.carbon.2012.10.039>
 35. Pavlets AS, Alekseenko AA, Tabachkova NY, Safronenko OI, Nikulin AY, Alekseenko DV, Guterman VE (2021) A novel strategy for the synthesis of Pt–Cu uneven nanoparticles as an efficient

- electrocatalyst toward oxygen reduction. *Int J Hydrogen Energy* 46:5255–5368. <https://doi.org/10.1016/j.ijhydene.2020.11.094>
36. Alekseenko AA, Ashihina EA, Shpanko SP, Volochaev VA, Safronenko OI, Guterman VE (2018) Application of CO atmosphere in the liquid phase synthesis as a universal way to control the microstructure and electrochemical performance of Pt/C electrocatalysts. *App Cat B* 226:608–615. <https://doi.org/10.1016/j.apcatb.2018.01.013>
 37. Brunauer S, Emmett PH, Teller E (1938) Adsorption of gases in multimolecular layers. *J Am Chem Soc* 60:309–319. <https://doi.org/10.1021/ja01269a023>
 38. Vidakovic T, Christov M, Sundmacher K (2007) The use of CO stripping for in situ fuel cell catalyst characterization. *Electrochim Acta* 52:5606–5613. <https://doi.org/10.1016/j.electacta.2006.12.057>
 39. Shinozaki K, Zack JW, Pylypenko S, Pivovar BS, Kocha SS (2015) Oxygen reduction reaction measurements on platinum electrocatalysts utilizing rotating disk electrode technique: II. Influence of ink formulation, catalyst layer uniformity and thickness. *J Electrochem Soc* 162:F1384. <https://doi.org/10.1149/2.0551512jes>
 40. Gasteiger HA, Kocha ShS, Sompalli B, Wagner FT (2005) Activity benchmarks and requirements for Pt, Pt-alloy, and non-Pt oxygen reduction catalysts for PEMFCs. *Appl Catal B* 56:9–35. <https://doi.org/10.1016/j.apcatb.2004.06.021>
 41. Khudhayer WJ, Kariuki NN, Wang X, Myers DJ, Shaikh AU, Karabacak T (2011) Oxygen reduction reaction electrocatalytic activity of glancing angle deposited platinum nanorod arrays. *J Electrochem Soc* 158:B1029–B1041. <https://doi.org/10.1166/asl.2011.1867>
 42. Maiyalagan T, Pasupathi S, Pollet BG (2015) The effects of cathode parameters on the performance of poly(2,5-Benzimidazole)-based polymer electrolyte membrane fuel cell. *Electrocatalysis* 6:155–162. <https://doi.org/10.1007/s12678-014-0228-8>
 43. Leontyev IN, Guterman VE, Pakhomova EB, Timoshenko PE, Guterman AV, Zakharchenko IN, Petin GP, Dkhil B (2010) XRD and electrochemical investigation of particle size effects in platinum–cobalt cathode electrocatalysts for oxygen reduction. *J Alloys Compd* 500:241–246. <https://doi.org/10.1016/j.jallcom.2010.04.018>
 44. Xiong Y, Ma Y, Zou L, Han Sh, Chen H, Wang Sh, Gu M, Shen Y, Zhang L, Xia ZH, Li J, Yang H (2020) N-doping induced tensile-strained Pt nanoparticles ensuring an excellent durability of the oxygen reduction reaction. *J Catal* 382:247–255. <https://doi.org/10.1016/j.jcat.2019.12.025>
 45. Luo Y, Kirchhoff B, Fantauzzi D, Calvillo L, Estudillo-Wong LA, Granozzi G, Jacob T, Alonso-Vante N (2017) Molybdenum doping augments platinum–copper oxygen reduction electrocatalyst. *ChemSusChem* 11:193–201. <https://doi.org/10.1002/cssc.201701822>
 46. Sing KSW, Everett DH, Haul RAW, Moscou L, Pierotti RA, Rouquerol J, Siemieniewska T (1985) Reporting physisorption data for gas/solid systems with special reference to the determination of surface area and porosity. *Pure Appl Chem* 57:603–619. <https://doi.org/10.1351/pac198557040603>
 47. Li Z, Jaroniec M (2001) Colloidal imprinting: a novel approach to the synthesis of mesoporous carbons. *J Am Chem Soc* 123:9208–9209. <https://doi.org/10.1021/ja0165178>
 48. Yamada Ya K, Yu M, Sh, Sato S (2014) Nitrogen-containing graphen analysed by X-ray photoelectron spectroscopy. *Carbon* 70:59–74. <https://doi.org/10.1016/j.carbon.2013.12.061>
 49. Weidenthaler C, Lu A-H, Shmidt W, Shuth F (2006) X-ray photoelectron spectroscopic studies of PAN-based ordered mesoporous carbons (OMC). *Microporous Mesoporous Mater* 88:238–243. <https://doi.org/10.1016/j.micromeso.2005.09.015>
 50. Orfanidi A, Madkikar P, El-Sayed HA, Harzer GS, Kratky T, Gasteiger HA (2017) The key to high performance low Pt loaded electrodes. *J Electrochem Soc* 164:F418–F426. <https://doi.org/10.1149/2.1621704je>
 51. Meier JC, Galeano C, Katsounaros I (2014) Design criteria for stable Pt/C fuel cell catalysts. *Beilstein J Nanotechnol* 5:44–67. <https://doi.org/10.3762/bjnano.5.5>
 52. Park YC, Kakinuma K, Uchida M, Uchida H, Watanabe M (2014) Deleterious effects of interim cyclic voltammetry on Pt/carbon black catalyst degradation during start-up/shutdown cycling evaluation. *Electrochim Acta* 123:84–92. <https://doi.org/10.1016/j.electacta.2013.12.120>
 53. Riese A, Banham D, Ye S, Sun X (2015) Accelerated stress testing by rotating disk electrode for carbon corrosion in fuel cell catalyst supports. *J Electrochem Soc* 162:F783. <https://doi.org/10.1149/2.0911507jes>
 54. Guterman VE, Belenov SV, Alekseenko AA, Rui Lin T, Tabachkova NY, Safronenko OI (2018) Activity and stability of Pt/C and Pt-Cu/C electrocatalysts. *Electrocatalysis* 9:550–562. <https://doi.org/10.1007/s12678-017-0451-1>

Publisher's Note Springer Nature remains neutral with regard to jurisdictional claims in published maps and institutional affiliations.

Authors and Affiliations

E. A. Moguchikh¹ · K. O. Paperzh¹ · A. A. Alekseenko¹ · E. N. Gribov^{2,3} · N. Yu. Tabachkova⁴ · N. V. Maltseva^{2,3} · A. G. Tkachev⁵ · E. A. Neskromnaya⁵ · A. V. Melezhik⁵ · V. V. Butova⁶ · O. I. Safronenko¹ · V. E. Guterman¹ 

✉ V. E. Guterman
guter@sfedu.ru; gut57@mail.ru

O. I. Safronenko
osafronenko@sfedu.ru

¹ Chemistry Faculty, Southern Federal University, 7 Zorge st., Rostov-on-Don, Russia 344090

² Boreskov Institute of Catalysis SB RAS, 5 Lavrentiev Ave., Novosibirsk, Russia 630090

³ Novosibirsk State University, 2 Pirogova st., Novosibirsk, Russia 630090

⁴ The Prokhorov Institute of General Physics, The Russian Academy of Sciences, 38 Vavilov st., Moscow, Russia 119991

⁵ NanoTechCentre LLC, 51 Sovetskaya st., 392000 Tambov, Russia

⁶ The Smart Materials Research Institute, Southern Federal University, 178/24 Sladkova st., Rostov-on-Don, Russia 344090